Ceramics-Silikáty 69 (2), 275-287 (2025)
www.ceramics-silikaty.cz doi: 10.13168/cs.2025.0012

THE RESISTANCE OF A PVA POWDER MODIFIED SULFOALUMINATE CEMENT CONCRETE TO THE CHLORIDE ION PERMEABILITY

SHUCHAO LV*, #YONGBO HUANG*, YONGJIE BIAN*, JIULONG LI**, PENGKUN HOU*, ***, PENG DU*, PIQI ZHAO*, SHOUDE WANG*

*Shandong Provincial Key Lab of Preparation and Measurement of Building Materials, University of Jinan, Jinan 250022, China
**Shandong high-speed traffic Construction Group, Jinan 250000, China
***School of Materials Science and Engineering, University of Jinan, Jinan 250022, China

#E-mail: 13589047192@163.com

Submitted December 10, 2024, accepted February 21, 2025

Keywords: Calcium sulfoaluminate cement, Polyvinyl alcohol powder, Chloride ion permeability, Capillary absorption coefficient, Pore structure

The transport rate of chloride ions (Cl^-) in sulfoaluminate cement (SAC) is lower than that in ordinary Portland cement (OPC). However, after long-term service, the steel rebar in the SAC still suffers erosion. To improve the chlorine ion erosion resistance of SAC concrete, this study incorporated a polyvinyl alcohol (PVA) powder into the SAC concrete. The effects of the PVA powder on the capillary absorption coefficient (S) and chloride ion erosion resistance of the specimen were evaluated. The results show that, after adding the PVA powder, the total porosity, macropores and capillary pores reduce. Meanwhile, the pore structure connectivity decreases and the pore complexity increases. The PVA powder decreases the capillary water absorption coefficient of the specimens (reduction rate > 21.84 %). Additionally, the electric flux and unsteady state chloride diffusion coefficient decrease by 16.32 % and 18.09 %, respectively, indicating that the transport rate of chloride ions inside the SAC concrete decreases and the chloride erosion resistance is improved. Therefore, the PVA powder-modified SAC concrete exhibits excellent resistance to chloride ion erosion, which becomes a good material for buildings with long service life requirements in marine engineering.

INTRODUCTION

Chloride ion erosion poses a great threat to concrete through the destruction of its alkaline environment, damaging the protective film surrounding the rebar and causing corrosion of the rebar. It leads to the formation of FeOOH which causes expansion and thereby induces concrete cracking. It is particularly pronounced in marine engineering [1-3], where chloride ion erosion has caused many structural durability failures and brought about safety concerns [4-5]. To solve the above issue, damaged concrete structures must undergo repair and reinforcement. Some countries allocate a substantial portion (40-50 %) of the budget to maintain and repair existing concrete buildings [6-7]. Additionally, from the perspective of the whole life cycle of the concrete buildings, the environmental burdens resulting from repair and reinforcement exceed those of the initial construction [8-9]. Consequently, improving the resistance of concrete to chloride ion erosion not only enhances the durability, but also decreases the environmental impact resulting from maintenance activities.

Sulfoaluminate cement (SAC) is a kind of environmentally-friendly and low-carbon cementitious materials, and the clinker is sintered at 1250-1350 °C [10]. The main mineral phases of the clinker include yelimite ($C_4A_3\$$), belite (C_2S) and celite (C_4AF) [11] and the main hydration products are ettringite (AFt), monosulfate (AFm), calcium silicate hydrate (C–S–H) gel and hydrated calcium aluminate [12]. SAC exhibits many performances, including high early age strength [13], fast hardening [14], low shrinkage [15], low porosity [16], and high corrosion resistance [17]. Therefore, it is widely applied in many engineering fields, which includes low-temperature construction, waterproofing, seepage resistance, marine engineering, and rapid repair [18-20]. The hydration products of SAC can absorb the Cl^- through chemical substitution (Cl^- can replace SO_4^- in AFm to form Friedel's Salt) and physical mechanisms (Cl^- is adsorbed physically by $Al(OH)_3$ and $Fe(OH)_3$ gels) [21–23]. Furthermore, the erosion products resulting from the chemical bonding of Cl^- effectively decrease the drying shrinkage and deformation, enhance the compactness of concrete, and inhibit the transport of Cl^- [24–26]. Therefore, SAC is frequently applied in marine engineering to extend the service life of buildings.

Many studies have proved that polymers could enhance the performances of cementitious material, particularly the bonding strength. These advantages make it promising in the application of concrete structural

repair and reinforcement [27-29]. At present, the types of polymers used to modify cementitious materials are re-dispersible powders, water-soluble polymer powders and polymer emulsions, including ethylene vinyl acetate powders [30], polyvinyl alcohol powders [31], butyl rubber emulsions [32] and so on. Due to its special chemical and physical properties, polyvinyl alcohol (PVA) has become one of the most widely used polymers. It is commonly used as a modifier, fibre reinforcing agent, pre-treatment for aggregate surfaces, and so on [33-35]. In the case of SAC, the inclusion of PVA fibres yields notable enhancements in the slurry rheology [36], toughness [37], and overall mechanical properties [38, 39], but only a few studies have focused on the durability [40], especially the resistance to chloride erosion. Moreover, most of the previous research focused on the influence of PVA powder on the properties of the mortar, but not concrete. The key is that concrete is the main load-bearing component and cannot be replaced by mortar. Therefore, it is necessary to study the effect of PVA powders on the properties of SAC concrete.

This study examines the influence of PVA powders on the chloride ion penetration resistance and its mechanism in SAC concrete to enhance the chloride erosion durability. Since water acts as the media for the migration of Cl^- inside the SAC concrete and the capillary absorption has close ties with the migration of water [41], this study evaluated the impact of PVA powders on the water absorption capacity of SAC by analysing the capillary water absorption coefficient. Additionally, the resistance of the PVA powder-modified SAC concrete to chloride ion permeation was evaluated by using the electric flux method, rapid chloride mobility coefficient (RCM) method, and natural diffusion method. Furthermore, the effects of Cl^- on the hydration products, pore structure, and microstructure of PVA powder-modified SAC concrete were also investigated. The findings of this study can help to prolong the service life of SAC concrete structures in marine environments.

Table 1. Physical parameters of the PVA powder.

Physical performance	Parameters
Molecular mass	17000 ~ 26000
Degree of polymerisation	500 ± 50
pH value	5.0 ~ 7.0
Viscosity (mpa·s)	4.5 ~ 6.5
Volatile content (%)	≤ 5.0
Ash content (%)	≤ 0.5
Purity (%)	≥ 96.0

EXPERIMENTAL

Raw materials

SAC is produced by China United Special Cement Co., Ltd., and the mineral compositions are shown in Figure 1. The cold-soluble PVA powder produced by Shanghai Yingjia Industrial Development Co., Ltd. was used and its main performance parameters are shown in Table 1. The medium sand was used as the fine aggregate, and limestone with the size of 5-16 mm was used as the coarse aggregate. The particle size distribution of the fine and coarse aggregates is shown in Table 2 and Table 3, respectively. The polycarboxylate superplasticiser with a 25 % solid content and 32 % water reducing rate was produced by Shandong Research Institute of Building Science Co., Ltd. Tributyl phosphate produced by ShangHai MacLean Biochemical Technology Co., Ltd. was used as the antifoam agent. Citric acid produced by Sinopharm Chemical Reagent Co., Ltd was used as the retarder.

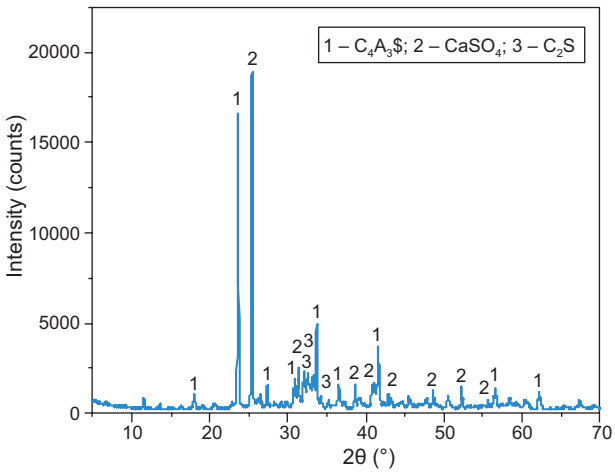

Figure 1. XRD pattern of the SAC.

Table 2. Size distribution of the fine aggregate.

Diameter	10 mm	5 mm	2.5 mm	1.25 mm	0.63 mm	0.32 mm	0.16 mm	Fineness modulus
Cumulative sieve residue (%)	0	1.42	14.21	30.34	52.87	75.31	92.95	2.62

Table 3. Size distribution of the coarse aggregate.

Diameter	20 mm	16 mm	10 mm	5 mm	2.5 mm	2.0 mm
Cumulative sieve residue (%)	0	3.75	52.94	89.87	99.89	0

Table 4. Specimen mixing ratio (kg·m^{-3}).

SAC	Water	Fine aggregate	Coarse aggregate	Water			PVA
				reducer (kg)	retarder (kg)	defoamer (kg)	
500	175	687	840	1.5	1.0	1.0	0 (0 %)
500	175	687	840	2.0	1.0	1.0	1.25 (0.25 %)
500	175	687	840	3.0	1.0	1.0	2.50(0.50 %)
500	175	687	840	4.3	1.0	1.0	3.75 (0.75 %)
500	175	687	840	6.5	1.0	1.0	5.00 (1.00%)

Sample preparation

The sample was prepared according to GB/T 50080-2016. The mixing proportion of SAC concrete was designed as shown in Table 4. With the increase in the PVA powder content, the slump-flow of concrete decreases. An amount of water-reducing agent was adjusted to ensure the good working performance of concrete. In this study, the slump flow of concrete is 650 mm.

Firstly, the PVA powder and SAC were mixed for at least 15 min. Secondly, the water reducer, retarder, and defoamer were added to the water. Finally, the coarse aggregate, fine aggregate, SAC and water were sequentially added to the mixer for 180 s. The size of the specimen is 100 × 100 × 100 mm. The specimens were cured in a standard curing room with a temperature of 20 ± 2 °C and a relative humidity of 95 % after moulding. After curing 1d, the specimens were demoulded.

Test methods

Capillary absorption coefficient

Specimens with a height 50 mm and diameter of 100 mm were used. After curing 28 days (28 day-curing), the specimens were dried to constant weight at 45 °C. The sides and upper surfaces of the specimens were sealed, and the lower surface was immersed in distilled water. Before the test, the initial weight of each specimen was measured.

The change of weight was calculated by Equation (1) in the progress of the capillary water absorption.

$$\mathrm{m}(t) = A\rho_1\varphi\sqrt{t\frac{r\gamma\cos\theta t}{2\eta}} \tag{1}$$

The amount of water absorption per unit area is per Equation (2).

$$I = \frac{m}{A\rho_1} = \varphi\sqrt{t\frac{r\gamma\cos\theta t}{2\eta}} = S\times\sqrt{t} \tag{2}$$

where A is the water contact area; ρ_1 is density of water; φ is the porosity of the sample; r is the pore radius; γ is the surface tension of the liquid; θ is the contact angle; η is the viscosity coefficient of water; S is the capillary water absorption coefficient.

The water absorption per unit area is linearly related to the square root of time, and the slope is the S.

Anti-chloride ions permeability

The electric flux method and RCM method detailed in GB/T 50082-2009 were used to test the anti-chloride ions permeability of the SAC concrete. The specimens, which had a height of 50 mm and a diameter of 100 mm were cured for 28 d before the tests. They were vacuum-encapsulated with water before testing.

When the electric flux method was used, a direct-current constant voltage of 60 V was applied to both ends of the fixture. The current value was recorded every 5 min for 6 hours. The total electric flux for each specimen was calculated using Equation (3):

$$Q = 900\,(I_0 + 2\,I_{30} + 2\,I_{60} + 2\,I_{30} + \ldots + 2\,I_t + \ldots + 2\,I_{300} + 2\,I_{330} + 2\,I_{360}) \tag{3}$$

where Q (Coulomb) is the total charge, I_0 is the ampere current generated immediately after the voltage is applied, and I_t is the ampere current after applying the voltage t min.

When the RCM method was used, the sample is fixed in the rubber sleeve. A 0.3 mol·L^{-1} NaOH solution and a 10 % mass concentration NaCl solution were added into the anode chamber and cathode chamber, respectively. The samples were separated by a cutter and sprayed with a 0.1 mol·L^{-1} $AgNO_3$ solution on the separation surface to determine the depth of penetration of Cl^-. The chloride ion diffusion coefficient was calculated using Equation (4).

$$D_{RCM} = \frac{0.0239\times(273+T)L}{(U-2)t}\left(d - 0.0238\sqrt{\frac{(273+T)Ld}{U-2}}\right) \tag{4}$$

where D_{RCM} is the non-steady state chloride ion migration coefficient with an accuracy of 0.1 × 10^{-12} m^2·s^{-1}; U is the absolute value of the applied voltage (V); T is the average value of the initial and end temperature in the anode solution (°C); L is the specimen thickness (mm) with an accuracy of 0.1 mm; X_d is the average value of the chloride ion penetration depth (mm) with an accuracy of 0.1 mm; t is the test time (h).

Pore structure

An automatic mercury intrusion meter (AutoPore V) was used to test the pore structure of the SAC concrete. The hydration of SAC was terminated with anhydrous ethanol. The samples were dried to constant weight at 45 °C before the test.

The fractal theories are widely used to study the pore structure of the hardened cementitious materials [42, 43]. Among the many fractal models, the model created by Baoquan Zhang et al. has proven to be more accurate and reliable in characterising the pore size distribution of concrete [44]. Based on the model, the fractal dimension is used to quantitatively describe the pore size distribution of concrete. The calculation formula is as follows:

$$\ln\left(\frac{W_n}{r_n^2}\right) = D_s \ln Q_n + \ln C \tag{5}$$

$$W_n = \sum_{i=1}^{n} P_i \Delta V_i \tag{6}$$

$$Q_n = \frac{\sqrt[3]{V_n}}{r_n} \tag{7}$$

where, W_n is the surface energy accumulated during the $n^{\text{-th}}$ mercury intrusion, r_n is the pore radius of mercury intrusion for the $n^{\text{-th}}$ mercury intrusion, V_n volume of mercury intrusion for the n-th mercury intrusion, D_s is pore surface fractal dimension, p_i is the pressure applied to the mercury injection at stage i *(Pa)*, ΔV_i is the volume of mercury injected into the pore at stage i (m^3), C is a constant, and n is the number of mercury injections during the mercury intrusion porosimetry (MIP) test.

X-ray diffraction (XRD) analysis

The samples were first crushed and immersed in anhydrous ethanol to cease the hydration. The samples were then dried and ground to pass through a 200 mesh (74 μm) sieve for X-ray diffraction (XRD). An XRD analysis of specimens was performed using a D8 ADVANCE X-ray diffractometer with Cu Kα radiation at 40 kV and 40 mA. A continuous scan was conducted over a 2θ range of 5°-70° with a step size of 0.02° and scan speed of 2°/min.

RESULTS AND DISCUSSION

Capillary water absorption coefficient

When the unsaturated concrete specimen is in the environment without differential pressure, water will enter it driven by the capillary force. After initial contact with water, the specimen will rapidly absorb the water.

Figure 2 shows the water absorption of the specimens with different amounts of PVA powder. The water absorption of the specimen increases with time before 500 h and keeps almost constant after 500 h. The water sorptivity decreases with the increase in the water absorption. The pore structure becomes dense due to the swelling of the C–S–H gel after the water absorption [45]. After adding the PVA powder, the water sorptivity of the specimen also decreases with the increase of the water absorption. It indicates that the PVA powder does not affect the swelling characteristics of the C–S–H gel after water absorption. When the capillary pores are saturated with water, the water gradually fills the large pores. Then, water transport is driven from capillary force to diffusion. Under the diffusion control, the water sorptivity of the specimen further decreased [46].

The influence of the dosage of the PVA powder on the total water absorption of the specimens at the hydration age of 28 d is shown in Figure 3. With the increase in the PVA powder content, the total water absorption of the specimens decreases. Previous investigations found that when PVAs are added to concrete, the small polymer particles can fill the partial micropores and voids. The part of the polymers interconnect to form a PVA polymer film, which can block or fill the pores [47]. Therefore, the concrete pores are refined and capillary forces are decreased after the addition of the PVA powder. It affects the water absorption process, which is mainly driven by

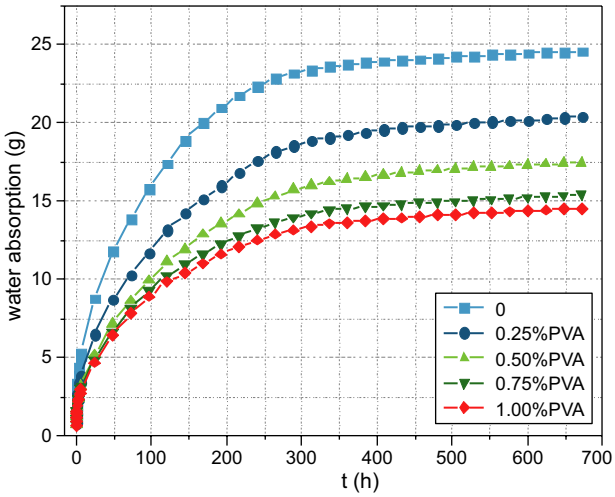

Figure 2. Water absorption of specimens with different amounts of PVA.

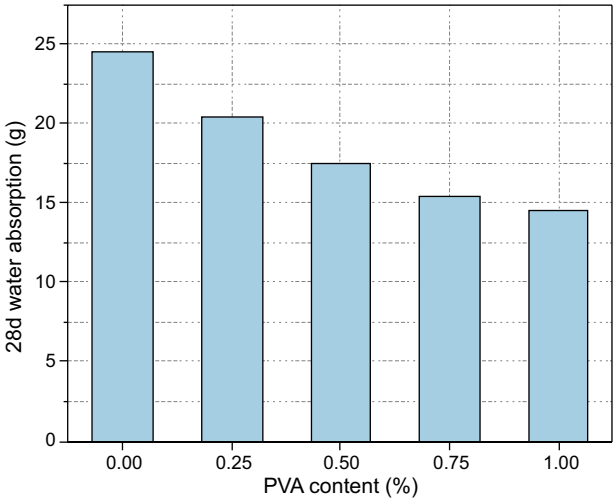

Figure 3. Influence of the dosage of PVA powder on the total water absorption of the specimens at the hydration age of 28 d.

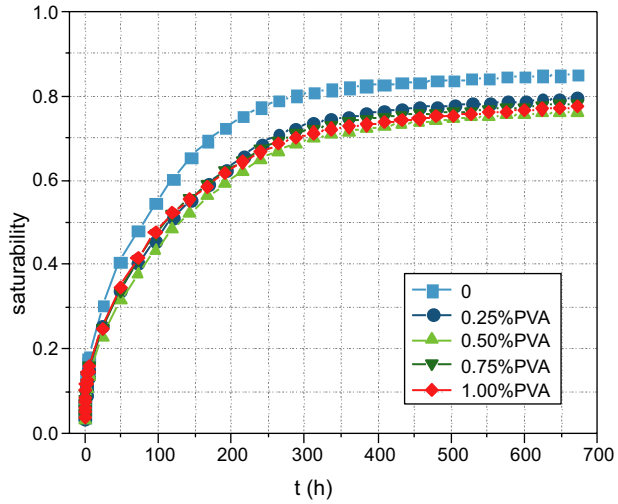

Figure 4. Effect of the dosage of the PVA powder on the saturation of the specimens.

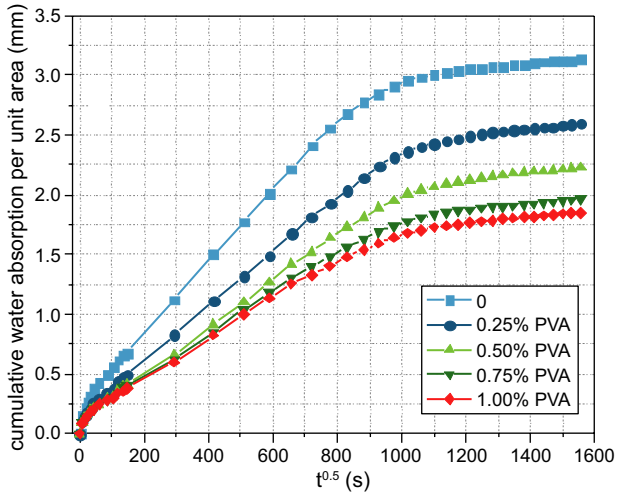

Figure 5. Influence of the PVA powder content on the cumulative water absorption per unit area of the specimen.

capillary forces. With the increase in the PVA powder content, the polymer film becomes more continuous and the blocking effect on pores is more obvious, which leads to a decrease in the water absorption.

The ratio of the water content inside a porous material to the water content at the saturated state is called saturation. It is the basic variable that describes the amount of water in a cementitious material [48]. Figure 4 shows the influence of the dosage of the PVA powder on the saturation of specimens. The saturation of the specimens increases with time. The saturation of the specimen decreases with the incorporation of the PVA powder. Due to the water content of the specimen at the saturated state being a particular value, the saturation of the specimen is directly proportional to the water content at the unsaturated state. It also proves that the water absorption of the concrete decreases with the addition of the PVA powder. However, the saturation remains almost constant with the increasing PVA powder content. At the hydration of 28 d, the maximum saturation of the control group and the sample with PVA are approximately 0.85 and 0.78, respectively.

Figure 5 shows the relationship between the cumulative water absorption per unit area (on the vertical axis) and the square root of the amount of time (on the horizontal axis). The cumulative water absorption per unit area decreases with the PVA powder content. Before the sample reaches the water absorption saturation, the cumulative water absorption per unit area exhibits a strong linear correlation with the square root of absorption time, and the slope of the line is the capillary water absorption coefficient (S) [49, 50], as shown in Figure 6.

As shown in Figure 6, the S of the specimens exhibits a decreasing tendency after adding the PVA powder. It is also due to that the PVA polymer film decreases the pore connectivity. The decreasing rate slows down

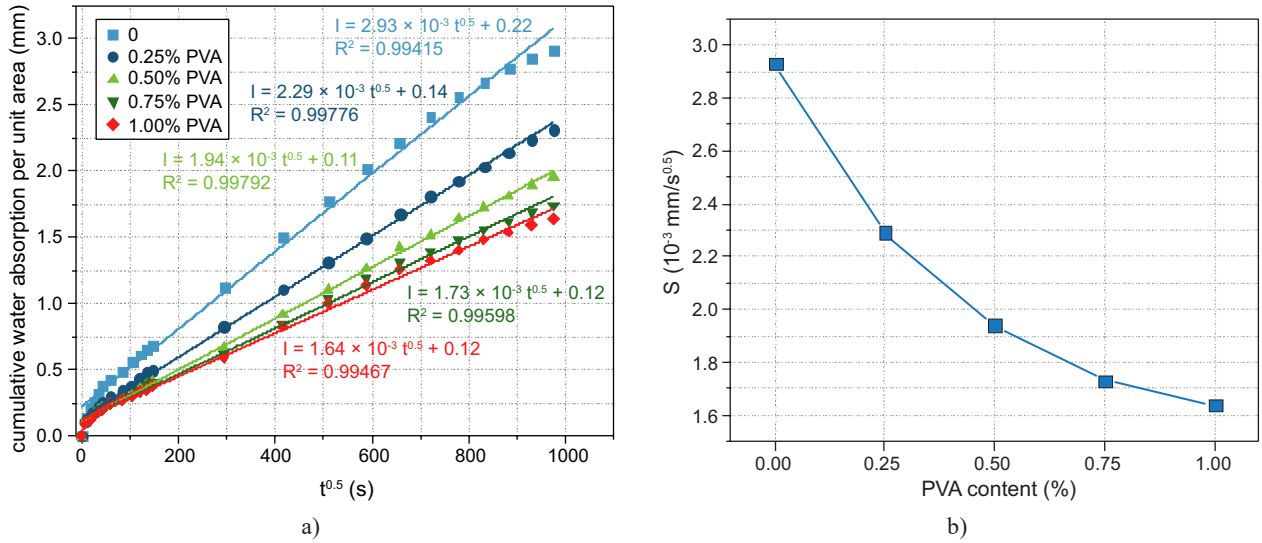

a) b)

Figure 6. Linear fitting results for the capillary water absorption of the specimen with different PVA powder contents (a); effect of the PVA powder content on the water absorption coefficient of the specimens (b).

when the PVA powder content exceeds 0.75 %, from 1.60×10^{-3} mm/s$^{0.5}$ to 1.57×10^{-3} mm/s$^{0.5}$. The decrease of the S of the specimen indicates that the water absorption is decreased, which is beneficial for the specimen to resist the penetration of aggressive ions [51].

Anti-chlorine permeability

Electric flux method

The chloride ions can move rapidly towards the positive electrode under the influence of direct current voltage. The ability of the specimen to resist the chloride ion penetration can be reflected by measuring the amount of electricity passed over a certain time [52]cementitious composites are exposed to a complex environment of coupled action of relative humidity, temperature, and chloride salts erosion, which severely impacts the safety and longevity of marine buildings. The effect of nano-SiO_2 dosage on the durability of polyvinyl alcohol fiber-reinforced cementitious composites (PVAF-RCC. The results are shown in Figure 7. From Figure7a, the electric current passing through the specimen increases with time, but decreases with an increase in the PVA powder content. The electrical flux of the specimens with 0 %, 0.25 %, 0.5 %, 0.75 %, 1 % PVA powder are 241 C, 202 C, 176 C, 162 C, 151 C in Figure 7b, respectively. As the PVA powder content increases, the electrical flux of the specimen continuously decreases. The low electrical flux indicates that the specimen has a good resistance to Cl^- [53]. Therefore, the electrical flux tests confirmed that the PVA powder can effectively improve the chloride ion penetration resistance of the concrete.

The Cl^- transport in the concrete primarily occurs through capillary action, infiltration, and diffusion, which are linked to the pore structure of concrete [46]. After adding the PVA powder, the polymer film could form in the internal voids of concrete, which thereby decreases the porosity of the concrete [56]. Additionally, the polymer film could also decrease the pore connectivity and hinder the formation of defects in the interfacial transition zone, which effectively impedes the diffusion and transport of Cl^- within the concrete [40]. Therefore, the PVA powder-modified specimens show excellent resistance to Cl^- permeability.

RCM method

The RCM method is based on the unsteady electromigration of chloride ions in the specimen [57]. Figure 8 shows the chloride ions penetration depth and the unsteady state chloride diffusion coefficient of the specimen. The penetration depth of chloride ions decreases with the increase in the PVA powder content. The chloride ions penetration depth of the specimen with 0 % and 1 % PVA powder are 27.6 mm and 13.8 mm, respectively. For the control group, the unsteady state chloride ion diffusion coefficient is 1.65×10^{-12} m^2·s^{-1}. The unsteady state chloride ion diffusion coefficient of the specimen with 1 % PVA powder decreases to 0.79×10^{-12} m^2·s^{-1}. As the PVA powder content increases, the unsteady state chloride ion diffusion coefficient of the specimen decreases. It is shown that the PVA powder-modified specimen has a much higher resistance to chloride ion penetration compared to the control specimen.

Effect of chloride ions on hydration products

The changes in the composition of the specimens before and after soaking in a 3.5 % NaCl solution are characterised by XRD, as shown in Figure 9. It shows that the intensity of the diffraction peaks of the calcium sulfoaluminate ($C_4A_3\$$) is weakened. However, the intensity of the diffraction peaks of the ettringite (AFt) is enhanced after the specimens are immersed in the NaCl

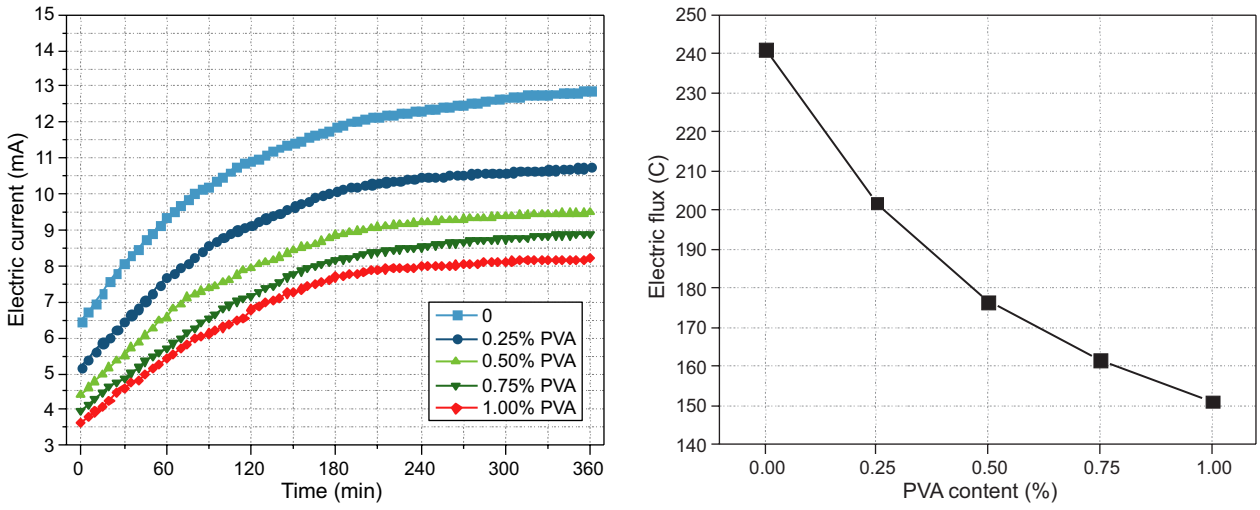

a) b)

Figure 7. Effect of the PVA powder dosage on the electric current (a) and electric flux (b) of the concrete.

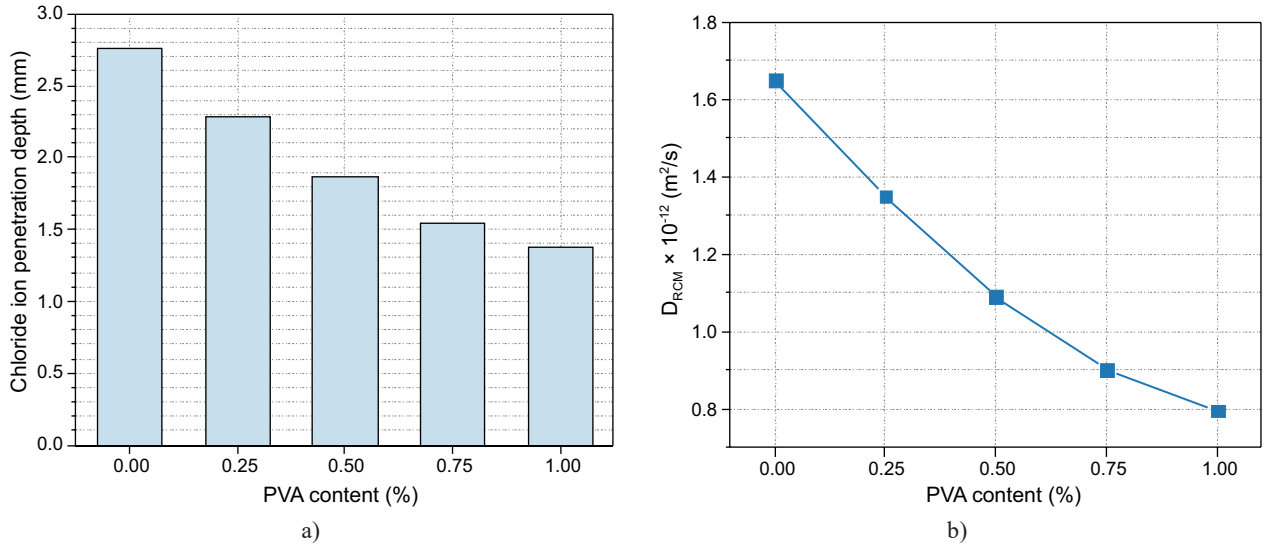

Figure 8. Effect of the dosage of the PVA powder on the chloride ion penetration depth (a) and unsteady state chloride ion diffusion coefficient (b) of the specimens.

solution for 90 d. It is due to that the penetrating water promotes the hydration reaction of the $C_4A_3\$$.

After adding the PVA powder, the diffraction peak intensity of the AFt of the unsoaked specimen increases. It benefits from the high carboxylate-charged polymers, such as the PVA powder, which enhance the hydration of $C_4A_3\$$ [58]. Nevertheless, after soaking in a NaCl solution for 90 d, the quantity of the hydration products of the specimens with different PVA powder content is the same. This can be attributed to that $C_4A_3\$$ is fully hydrated after soaking in a NaCl solution, decreasing the influence of the PVA powder on the hydration of $C_4A_3\$$.

After soaking in 3.5 % NaCl solution for 90 d, a small quantity of Friedel's salt is found. It is due to the fact that AFt can react with chloride ions to form Friedel's salt [59]. Moreover, the excellent impermeability of the specimen allows a small amount of Cl^- to penetrate.

Effect of chloride ions on the pore structure

The porosity, pore size distribution and pore connectivity are the important parameters that affect the permeability of concrete [60]. Polymers can form polymer films in the pores of concrete, which reduces the pore connectivity and affects the pore size distribution [47]. The porosity and pore size distribution of the specimen after soaking in a 3.5 % NaCl solution are shown in Figure 10. It shows that the PVA powder decreases the porosity of the specimens.

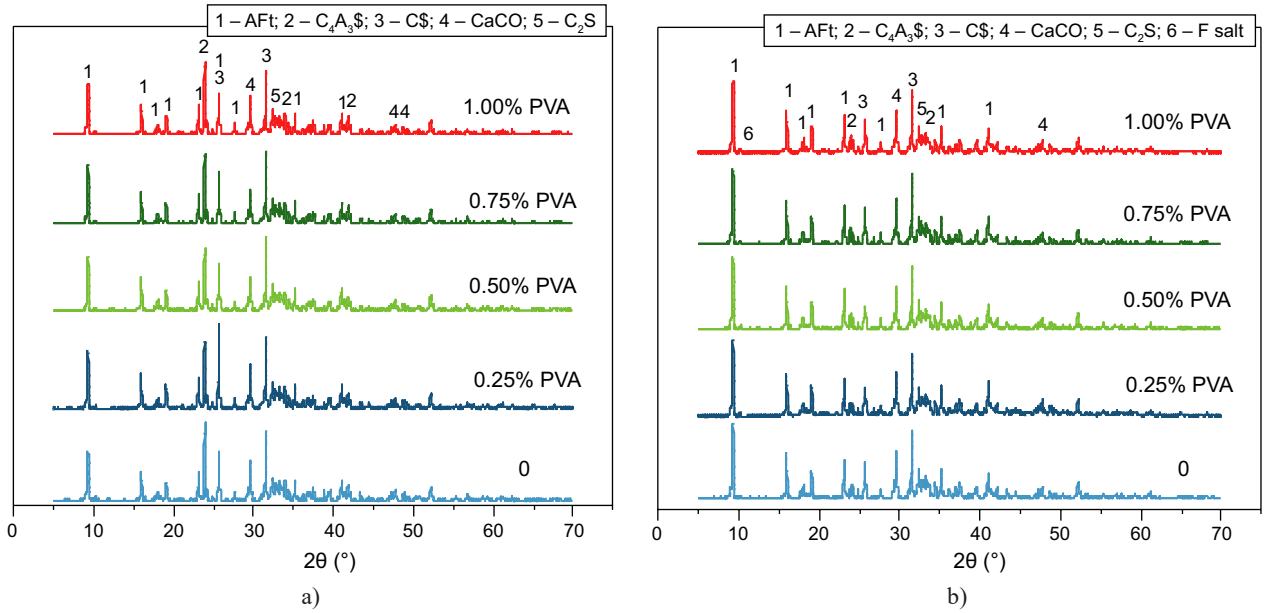

Figure 9. XRD patterns of specimens before (a) and after (b) soaking in a 3.5 % NaCl solution.

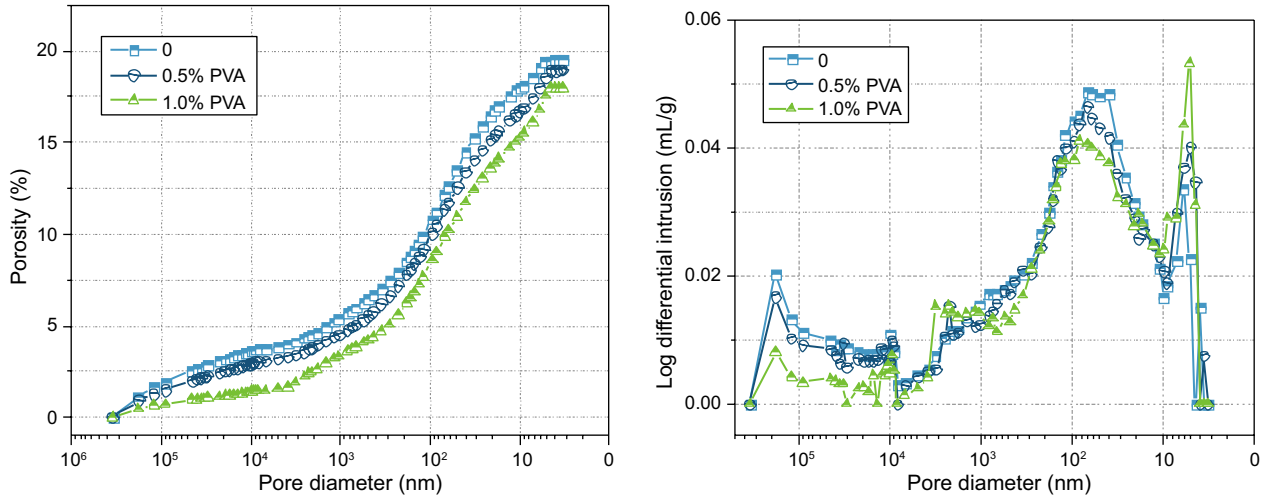

Figure 10. Porosity (a) and pore size distribution (b) of the specimens after soaking in a 3.5% NaCl solution for 90 d.

The percentage of the pore size distribution after soaking in a 3.5 % NaCl solution is shown in Figure 11. The percentages of gel pores, capillary pores and macropores of the control specimen are 1.54 %, 12.61 % and 5.36 %, respectively. The percentage distributions are 2.27 %, 12.18 %, and 4.52 % for the specimens with the 0.5% PVA powder and 2.68 %, 11.87 %, and 3.34 % for the specimens with the 1 % PVA powder, respectively. It can be seen that the porosity decreases with the increase in the PVA powder. This results in a decrease in the proportion of capillary pores and macropores and an increase in gel pores. As mentioned earlier, both the filling effect of small particles of the PVA and the blocking effect of the PVA polymer film decrease the porosity of the concrete.

Water is an important medium for Cl^- erosion. It is transported in concrete as a gas or liquid. The interconnected gel pores, capillary pores, and macropores can be used as channels for water transport. The addition of the PVA powder increases the number of gel holes. However, the gel holes do not have a negative effect on the properties of concrete. The proportion of capillary pores and macropores decreases with the addition of the PVA powder. It reduces the water transport channels, which can further decrease the Cl^- content that intrudes into the concrete. It indicates that the PVA powder has a positive effect on the chloride ion erosion resistance of concrete.

Figure 12 and Figure 13 show the porosity and pore size distribution of the specimens before and after soaking in a 3.5 % NaCl solution, respectively. After soaking in a 3.5 % NaCl solution for 90 d, the porosity of the control specimen decreases by 1.93 %. The porosity of the specimen with 0.5 % and 1.0 % PVA powder merely decreases by 0.11 % and 0.17 %, respectively.

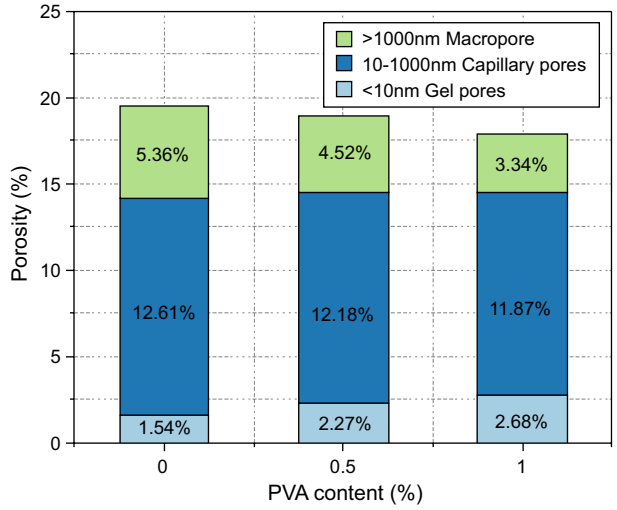

Figure 11. Proportion of specimen pore size after soaking in a 3.5 % NaCl solution for 90 d.

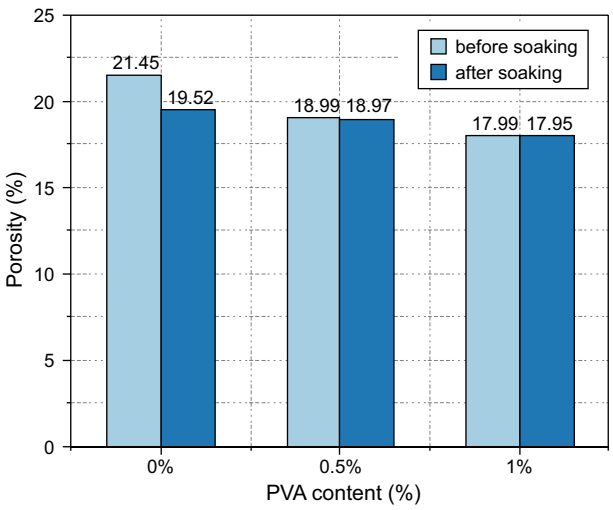

Figure 12. Porosity of the specimens before and after immersion in a 3.5 % NaCl solution for 90 d.

For the control group, Cl^- intruded into concrete under water transportation when soaking in a 3.5 % NaCl solution. The AFt generated by the further hydration of $C_4A_3\$$ enhances the compaction of concrete. Additionally, AFt reacts with Cl^- to form Friedel's salt, further contributing to the pore structure densification.

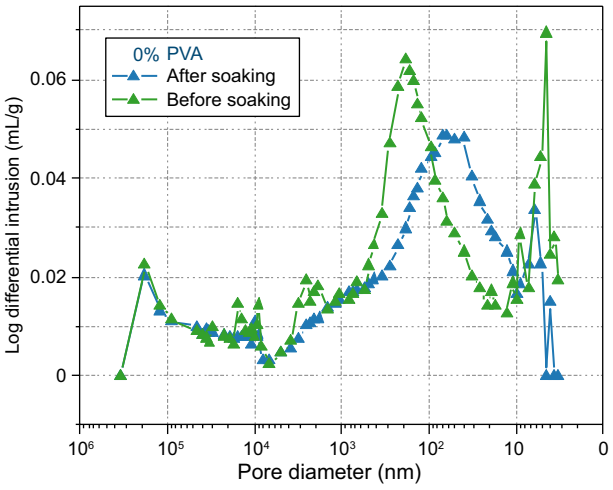

a)

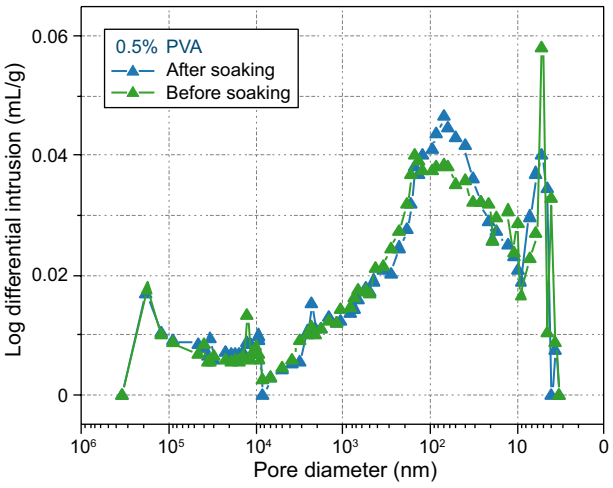

a)

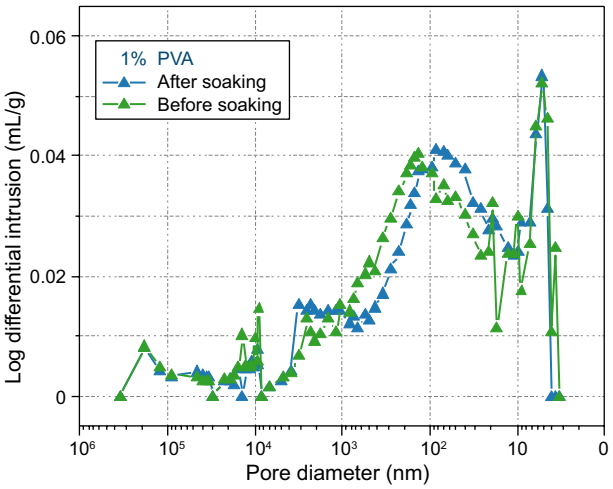

b)

Figure 13. Pore size distribution of the specimens before and after immersion in an NaCl solution for 90 d.

The porosity of the specimen with the addition of the PVA powder changes slightly after soaking in a 3.5 % NaCl solution. On the one hand, the addition of the PVA powder promoted the hydration of $C_4A_3\$$. On the other hand, the PVA molecules are interconnected to form a polymer film inside the concrete, which hinders the diffusion and transport of the water and Cl^-.

The critical pore size of the pore structure is an important parameter that characterises the connectivity of concrete pores. Only pores equal to or smaller than critical pore size can be interconnected [61]. Figure 14 shows the critical pore size of the specimens before and after soaking in a 3.5 % NaCl solution. After soaking in a 3.5 % NaCl solution, the critical pore size of all the specimens decreased. It is due to the fact that the AFt formed by the hydration of $C_4A_3\$$ and the Friedel's salt formed by the combination of Cl^- with AFt can densify the pore structure of the specimen. Therefore, the critical pore size of the specimen also decreases.

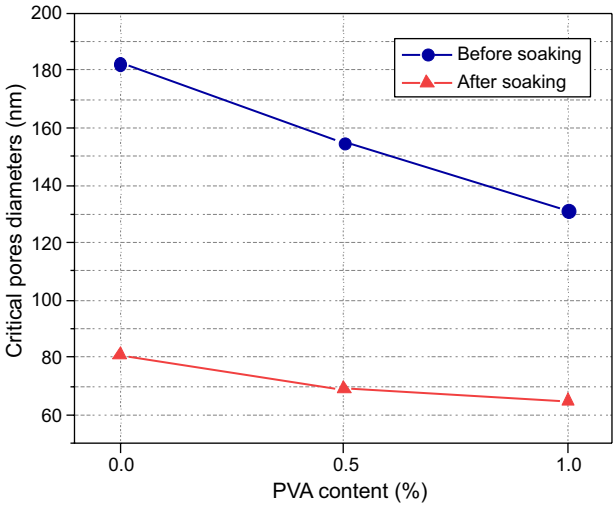

Figure 14. Critical pore size of the specimen before and after soaking in a 3.5 % NaCl solution.

Baoquan Zhang et al. proposed that the fractal dimension is used to quantitatively describe the pore structure of concrete. A larger value of the fractal dimension represents the higher complexity of the concrete pore structure [62]. The fractal dimensions of the specimens before and after soaking in a 3.5 % NaCl solution are shown in Figure 15. After soaking in a 3.5 % NaCl solution, the fractal dimension of the control specimen increases. The fractal dimension of the specimen with the 0.5 % PVA powder is almost unchanged, but the fractal dimension of the specimen with the 1 % PVA powder decreases.

After soaking in a 3.5 % NaCl solution, the pore size of the control specimen is further refined and the pore structure becomes more complex. For the specimens

with the addition of the PVA powder, the PVA powder promotes the hydration of $C_4A_3\$$. Additionally, the PVA polymer film formed by the interconnection of PVA molecules hinders the transport and diffusion of water and Cl^-. It means that the pore structure of the specimen with the PVA powder changes a little after immersion. As a result, the fractal dimension of the specimen increases a little.

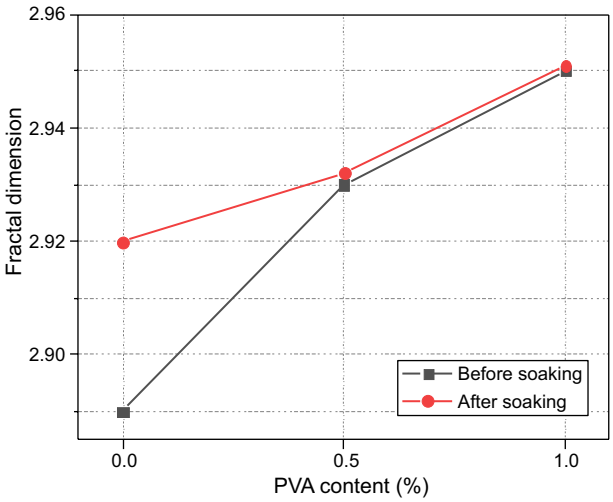

Figure 15. Fractal dimension of the specimen before and after immersion in a 3.5 % NaCl solution.

The pore connectivity of the specimen before and after soaking in a 3.5 % NaCl solution is shown in Figure 16. After immersion, the pore connectivity of all the specimens decreases. However, the decrease in sample size with the addition of PVA powder is negligible. Because the critical pore diameter is an important parameter to characterise the connectivity of concrete pore structures. The change pattern of pore connectivity of the specimen is the same as that of the critical pore diameter. Therefore, it is consistent with the conclusion given in Figure 14.

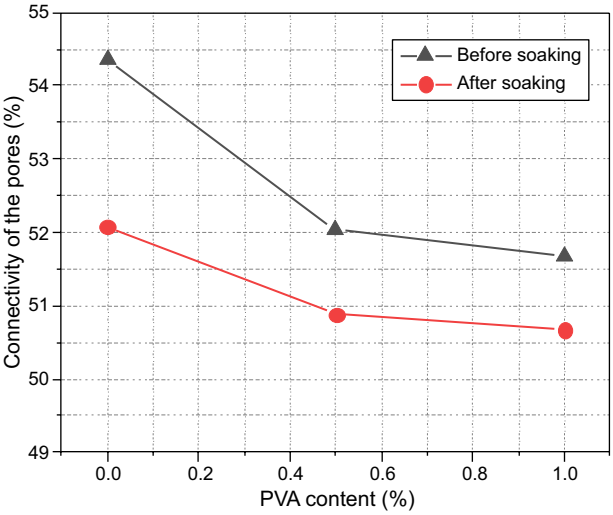

Figure 16. Pore connectivity of specimens before and after soaking in the NaCl solution.

CONCLUSIONS

This paper introduces the use of PVA to improve the resistance of Cl^- erosion in SAC concrete, and the results show that PVA has a promising effect. Test samples were prepared with various additions of PVA. Based on the test results, the following conclusions can be drawn:

- The addition of PVA decreases the capillary water absorption coefficient of the specimen. The capillary water absorption coefficient of concrete decreases from 2.93×10^{-3} mm/s$^{0.5}$ to 1.64×10^{-3} mm/s$^{0.5}$ with the content of PVA powder from 0 to 1 %.
- The PVA powder improves the resistance of the specimens to chloride ion permeability. With the content of PVA powder changing from 0 to 1 %, the electrical flux of the concrete decreases from 241 C to 151 C and the non-steady state chloride ion diffusion coefficient of the concrete decreases from 1.65×10^{-12} m^2/s to 0.79×10^{-12} m$^2\cdot$s^{-1}.
- After soaking in a 3.5 % NaCl solution for 90 d, the hydration degree of SAC increases. Furthermore, AFt can combine with Cl^- to form Friedel's salt. The water that enters the specimen after immersion promotes the cement hydration process, which weakens the positive effect of the PVA powder on the cement hydration.
- The PVA powder can form a polymer film inside the concrete, and decrease the concrete porosity and connectivity, which positively affects the permeability of anti-chlorine ions. With the addition of PVA powder from 0 to 1 %, the concrete porosity decreased from 19.52 % to 17.95 % and the critical pore size decreased from 81.02 nm to 64.74 nm after immersion in the NaCl solution for 90 d.

Acknowledgement

The authors gratefully acknowledge the financial support from National Key Research and Development Program of China (2022YFE0208200), Natural Science Foundation of China (52372027), Science and Technology project of Inner Mongolia Autonomous Region (2023YFHH0085, 2022YFHH0118), Taishan Scholars Program (tsqnz20221144, tsqn202211170), Natural Science Foundation of Shandong Province (2023TSGC0973), Support Plan for Young Researchers in Institutes of Higher Education in Shandong.

REFERENCES

1. Tang S. W., Yao Y., Andrade C., Li Z. J. (2015): Recent durability studies on concrete structure. *Cement and Concrete Research*, *78*, 143-154. doi:10.1016/J.CEMCONRES.2015.05.021
2. Shang H., Yang J., Huang Y., Fan L., Wang R. (2022): Study on the bond behavior of steel bars embedded in concrete under the long-term coupling of repeated loads and chloride ion erosion. *Construction and Building Materials*, *323*, 126498. doi: 10.1016/J.CONBUILDMAT.2022.126498

3. Hou D., Zhang K., Hong F., Wu S., Wang Z., Li M., Wang M. (2022): The corrosion deterioration of reinforced passivation Film: The impact of defects. *Applied Surface Science*, *582*, 152408. doi: 10.1016/J.APSUSC.2021.152408
4. Hosseinzadeh N., Ghiasian M., Andiroglu E., Lamere J., Rhode-Barbarigos L., Set al. (2022): Concrete seawalls: A review of load considerations, ecological performance, durability, and recent innovations. *Ecological Engineering*, *178*, 106573. doi: 10.1016/j.ecoleng.2022.106573
5. Baloch W. L., Siad H., Lachemi M., Sahmaran M. (2021): A review on the durability of concrete-to-concrete bond in recent rehabilitated structures. *Journal of Building Engineering*, *44*, 103315. doi: 10.1016/j.jobe.2021.103315
6. Zhou J., Ye G., van Breugel K. (2016): Cement hydration and microstructure in concrete repairs with cementitious repair materials. *Construction and Building Materials*, *112*, 765-772. doi: 10.1016/j.conbuildmat.2016.02.203
7. Polder R. B., Peelen W. H. A., Courage W. M. G. (2012): Non-traditional assessment and maintenance methods for aging concrete structures –t echnical and non-technical issues. *Materials and Corrosion*, *63*(12), 1147-1153. doi: 10.1002/maco.201206725
8. Alexander M., Beushausen H. (2019): Durability, service life prediction, and modelling for reinforced concrete structures – review and critique. *Cement and Concrete Research*, *122*, 17-29. doi: 10.1016/j.cemconres.2019.04.018
9. Mehta P. K., Monteiro P. (2006). *Concrete: microstructure, properties, and materials.* McGraw-Hill.
10. Chen T., Wang Z., Bai E., Wang A., Luo X. (2023): Effect of nano admixtures on the engineering properties and microstructure of sulphoaluminate cement mortar at − 10 C. *Construction and Building Materials*, *402*, 133015. doi: 10.1016/j.conbuildmat.2023.133015
11. Guo C., Wang R. (2023): Using sulphoaluminate cement and calcium sulfate to modify the physical – chemical properties of Portland cement mortar for mechanized construction. *Construction and Building Materials*, *367*, 130252. doi: 10.1016/j.conbuildmat.2022.130252
12. Li J., Wang R., Xu Y. (2022): Influence of cellulose ethers chemistry and substitution degree on the setting and early-stage hydration of calcium sulphoaluminate cement. *Construction and Building Materials*, *344*, 128266. doi:10.1016/j.conbuildmat.2022.128266
13. Bi R., Cheng W., Chen X. (2019): Effect of calcium sulfate variety and content on hydration mechanism of grout sealants for coal-bed methane drainage boreholes. *Construction and Building Materials*, *203*, 443-455. doi: 10.1016/j.conbuildmat.2019.01.046
14. Deng X., Guo H., Tan H., Zhang J., et al. (2022): Comparison on early hydration of Portland cement and sulphoaluminate cement in the presence of nano ettringite. *Construction and Building Materials*, *360*, 129516. doi: 10.1016/j.conbuildmat.2022.129516
15. Ke G., Zhang J., Liu Y. (2022): Shrinkage characteristics of calcium sulphoaluminate cement concrete. *Construction and Building Materials*, *337*, 127627. doi: 10.1016/j.conbuildmat.2022.127627
16. Zhang L., Glasser F. P. (2005): Investigation of the microstructure and carbonation of CS^{-} A-based concretes removed from service. *Cement and Concrete Research*, *35*(12), 2252-2260. doi: 10.1016/j.cemconres.2004.08.007
17. Juenger M. C. G., Winnefeld F., Provis J. L., Ideker J. H. (2011): Advances in alternative cementitious binders. *Cement and concrete research*, *41*(12), 1232-1243. doi: 10.1016/j.cemconres.2010.11.012
18. Gartner E., Sui T. (2018): Alternative cement clinkers. *Cement and Concrete Research*, *114*, 27-39. doi: 10.1016/j.cemconres.2017.02.002
19. Yu L., Bi H., Wang Z., Wu F., et al. (2023): Feasibility of using iron-rich phosphoaluminate cement to prepare anticorrosive coatings for rebars. *Construction and Building Materials*, *401*, 132736. doi: 10.1016/j.conbuildmat.2023.132736
20. Haque M. A., Chen B. (2019): Research progresses on magnesium phosphate cement: A review. *Construction and building materials*, *211*, 885-898. doi: 10.1016/j.conbuildmat.2019.03.304
21. Li G., Zhang J., Song Z., Shi C., Zhang A. (2018): Improvement of workability and early strength of calcium sulphoaluminate cement at various temperature by chemical admixtures. *Construction and Building Materials*, *160*, 427-439. doi: 10.1016/j.conbuildmat.2017.11.076
22. Abir F. Z., Mesnaoui M., Abouliatim Y., Nibou L., Labbilta T., et al. (2022): Effect of the addition of iron oxide on the microstructure of ye'elimite. *Cement and Concrete Research*, *151*, 106625. doi: 10.1016/j.cemconres.2021.106625
23. Jia F., Sun H., Yu L., Lu X., Zhou Y., Elchalakani M., Du P. (2023): Effects of different gypsum varieties on the hydration and mechanical properties of red mud-based ferrite-rich sulfoaluminate cement. *Journal of Materials Research and Technology*, *24*, 3086-3097. doi: 10.1016/j.jmrt.2023.03.197
24. Wu F., Bi H., Lin H., Wang X., et al. (2023): Physical and chemical chloride binding characteristics of the hydration products for phosphoaluminate cement. *Construction and Building Materials*, *403*, 133044. doi: 10.1016/j.conbuildmat.2023.133044
25. Martın-Pérez B., Zibara H., Hooton R. D., Thomas M. D. A. (2000): A study of the effect of chloride binding on service life predictions. *Cement and concrete research*, *30*(8), 1215-1223. doi: 10.1016/S0008-8846(00)00339-2
26. Brown P., Bothe Jr J. (2004): The system $CaO-Al_2O_3-CaCl_2-H_2O$ at 23±2 C and the mechanisms of chloride binding in concrete. *Cement and Concrete Research*, *34*(9), 1549-1553. doi: 10.1016/j.cemconres.2004.03.011
27. Sun K., Wang S., Zeng L., Peng X. (2019): Effect of styrene-butadiene rubber latex on the rheological behavior and pore structure of cement paste. *Composites Part B: Engineering*, *163*, 282-289. doi: 10.1016/j.compositesb.2018.11.017
28. Pang B., Jia Y., Dai Pang S., Zhang Y., et al. (2021): The interpenetration polymer network in a cement paste – waterborne epoxy system. *Cement and Concrete Research*, *139*, 106236. doi: 10.1016/j.cemconres.2020.106236
29. Yao H., Fan M., Huang T., Yuan Q., et al. (2021): Retardation and bridging effect of anionic polyacrylamide in cement paste and its relationship with early properties. *Construction and Building Materials*, *306*, 124822. doi: 10.1016/j.conbuildmat.2021.124822
30. Sh, C., Zou X., Wang P. (2018): Influences of ethylene-vinyl acetate and methylcellulose on the properties of calcium sulfoaluminate cement. *Construction and Building Materials*, *193*, 474-480. doi: 10.1016/j.conbuildmat.2018.10.218
31. Allahverdi A., Kianpur K., Moghbeli M. R. (2010): Effect of polyvinyl alcohol on flexural strength and some important physical properties of Portland cement paste. *Iran. J. Mater. Sci. Eng*, *7*(1), 1-6.

32. Zhang C., Wang J., Zhang S., Hou X., Kong X. (2024): Damping performance of hardened cement pastes containing styrene-butyl acrylate polymers with varied glass transition temperature and surface charges. *Cement and Concrete Composites*, *145*, 105312. doi: 10.1016/j.cemconcomp.2023.105312
33. Thong C. C., Teo D. C. L., Ng C. K. (2016): Application of polyvinyl alcohol (PVA) in cement-based composite materials: A review of its engineering properties and microstructure behavior. *Construction and Building Materials*, *107*, 172-180. doi: 10.1016/j.conbuildmat.2015.12.188
34. Liu F., Xu K., Ding W., Qiao Y., Wang L. (2021): Microstructural characteristics and their impact on mechanical properties of steel-PVA fiber reinforced concrete. *Cement and Concrete Composites*, *123*, 104196. doi: 10.1016/j.cemconcomp.2021.104196
35. Zárybnická L., Mácová P., Viani A. (2022): Properties enhancement of magnesium phosphate cement by cross-linked polyvinyl alcohol. *Ceramics International*, *48*(2), 1947-1955. doi: 10.1016/j.ceramint.2021.09.279
36. Chen M., Yang L., Zheng Y., Li L., et al. (2021): Rheological behaviors and structure build-up of 3D printed polypropylene and polyvinyl alcohol fiber-reinforced calcium sulphoaluminate cement composites. *Journal of Materials Research and Technology*, *10*, 1402-1414. doi: 10.1016/j.jmrt.2020.12.115
37. Li J., Yan J., Xue G., Niu J. (2021): Acoustic emission behavior of polyvinyl alcohol (PVA) fiber reinforced calcium sulphoaluminate cement mortar under flexural load. *Journal of Building Engineering*, *40*, 102734. doi: 10.1016/j.jobe.2021.102734
38. Li Y., Li W., Deng D., Wang K., Duan W. H. (2018): Reinforcement effects of polyvinyl alcohol and polypropylene fibers on flexural behaviors of sulfoaluminate cement matrices. *Cement and Concrete Composites*, *88*, 139-149. doi: 10.1016/j.cemconcomp.2018.02.004
39. Xue W., Wang Z., Alam M. S., Xu L., Xu J. (2023): Mechanical and seepage characteristics of polyvinyl alcohol fiber concrete under stress-seepage coupling. *Journal of Building Engineering*, *78*, 107694. doi: 10.1016/j.jobe.2023.107694
40. Dong D., Huang Y., Gao X., Bian Y., et al. (2023): Effect of polyvinyl alcohol powder on the impermeability, frost resistance and pore structure of calcium sulfoaluminate cement concrete. *Construction and Building Materials*, *409*, 133858. doi: 10.1016/j.conbuildmat.2023.133858
41. Medeiros M. H., Helene P. R. D. L. (2009): Surface treatment of reinforced concrete in marine environment: Influence on chloride diffusion coefficient and capillary water absorption. *Construction and Building Materials*, *23*(3), 1476-1484. doi: 10.1016/j.conbuildmat.2008.06.013
42. Wang J., Wang X., Ding S., Ashour A., Yu F., Lv X., Han B. (2023): Micro-nano scale pore structure and fractal dimension of ultra-high performance cementitious composites modified with nanofillers. *Cement and Concrete Composites*, *141*, 105129. doi: 10.1016/j.cemconcomp.2023.105129
43. Wang L., Jin M., Wu Y., Zhou Y., Tang S. (2021): Hydration, shrinkage, pore structure and fractal dimension of silica fume modified low heat Portland cement-based materials. *Construction and Building Materials*, *272*, 121952. doi: 10.1016/j.conbuildmat.2020.121952
44. Zhang B., Liu W., Liu X. (2006): Scale-dependent nature of the surface fractal dimension for bi-and multi-disperse porous solids by mercury porosimetry. *Applied Surface Science*, *253*(3), 1349-1355. doi: 10.1016/j.apsusc.2006.02.009
45. Zheng S., Chen H., Xiao Y., He R., Qiu H. (2024): Water distribution characteristics of capillary absorption in internally cured concrete with superabsorbent polymers. *Construction and Building Materials*, *418*, 135446. doi: 10.1016/j.conbuildmat.2024.135446
46. Li S. S., Liu H., Bharath M. S., Zhang S. X., Cheng X. (2020): Variation in the sulfate attack resistance of iron rich-phosphoaluminate cement with mineral admixtures subjected to a Na_2SO_4 solution. *Construction and Building Materials*, *230*, 116817. doi: 10.1016/J.CONBUILDMAT.2019.116817
47. Knapen E., Van Gemert D. (2009): Cement hydration and microstructure formation in the presence of water-soluble polymers. *Cement and Concrete Research*, *39*(1), 6-13. doi: 10.1016/j.cemconres.2008.10.003
48. Ren F., Zhou C., Zeng Q., Ding Z., Xing F., Wang W. (2019): The dependence of capillary sorptivity and gas permeability on initial water content for unsaturated cement mortars. *Cement and Concrete Composites*, *104*, 103356. doi: 10.1016/j.cemconcomp.2019.103356
49. Zhang C., Zhang S., Yu J., Kong X. (2022): Water absorption behavior of hydrophobized concrete using silane emulsion as admixture. *Cement and Concrete Research*, *154*, 106738. doi: 10.1016/j.cemconres.2022.106738
50. Wang Y., Wang W., Wang D., Liu Y., Liu J. (2021): Study on the influence of sample size and test conditions on the capillary water absorption coefficient of porous building materials. *Journal of Building Engineering*, *43*, 103120. doi: 10.1016/j.jobe.2021.103120
51. El Abd A., Taman M., Kichanov S. E., Hamad E., Nazarov K. M. (2021): Implementation of capillary penetration coefficient on water sorptivity for porous building materials: An experimental study. *Construction and Building Materials*, *298*, 123758. doi: 10.1016/j.conbuildmat.2021.123758
52. Wang C., Zhang P., Guo J., Wang J., Zhang T. (2023): Durability and microstructure of cementitious composites under the complex environment: Synergistic effects of nano-SiO_2 and polyvinyl alcohol fiber. *Construction and Building Materials*, *400*, 132621. doi: 10.1016/j.conbuildmat.2023.132621
53. Zhang G., Chen H., Yang J., Ding Q., Li Y., Wang Y. (2023): Relationship between chloride ion permeation resistance of ultra-high performance concrete and lightweight aggregate ratio. *Journal of Building Engineering*, *76*, 107360. doi: 10.1016/j.jobe.2023.107360
54. Lu L., Yang Z., Lin Y., Dong S. (2023): Partial replacement of manufactured sand with homologous granite powder in mortar: The effect on porosity and capillary water absorption. *Construction and Building Materials*, *376*, 131031. doi: 10.1016/j.conbuildmat.2023.131031
55. Zhu C., Liu X., Liu C., Yu W., Bai G. (2022): Study on the chloride ion transport mechanism of recycled mixed aggregate concrete based on evolution characteristics of pore structure. *Construction and Building Materials*, *353*, 129101. doi: 10.1016/j.conbuildmat.2022.129101
56. Li G., Wang L., Yu J., Yi B., He C., Wang Z., Leung C. K. (2022): Mechanical properties and material characterization of cement mortar incorporating CNT-engineered polyvinyl

alcohol latex. *Construction and Building Materials*, *345*, 128320. doi: 10.1016/j.conbuildmat.2022.128320

57. Luo X., Huang X., Liu Y., Tao J., Xiao S., Peng B. (2023): Performance characterization and optimization of cement-lithium powder-grain slag composite cementitious materials. *Construction and Building Materials*, *409*, 133851. doi: 10.1016/j.conbuildmat.2023.133851
58. Lu Z., Kong X., Zhang C., Cai Y. (2018): Effect of highly carboxylated colloidal polymers on cement hydration and interactions with calcium ions. *Cement and Concrete Research*, *113*, 140-153. doi: 10.1016/j.cemconres.2018.08.010
59. Florea M. V. A., Brouwers H. J. H. (2012): Chloride binding related to hydration products: Part I: Ordinary Portland Cement. *Cement and Concrete Research*, *42*(2), 282-290. doi: 10.1016/j.cemconres.2011.09.016
60. Bagel L., Živica V. (1997): Relationship between pore structure and permeability of hardened cement mortars: on the choice of effective pore structure parameter. *Cement and Concrete Research*, *27*(8), 1225-1235. doi: 10.1016/S0008-8846(97)00111-7
61. Atahan H. N., Oktar O. N., Taşdemir M. A. (2009): Effects of water–cement ratio and curing time on the critical pore width of hardened cement paste. *Construction and Building materials*, *23*(3), 1196-1200. doi: 10.1016/j.conbuildmat.2008.08.011
62. Zhu D., Zhu S., Tang A. (2023): Effect of clinoptilolite on properties and fractal characteristic of pore structure of polypropylene fiber-reinforced cement-based composite. *Construction and Building Materials*, *402*, 132964. doi: 10.1016/j.conbuildmat.2023.132964